

Femtosecond near-field spectroscopy: carrier relaxation and transport in single quantum wires

V. EMILIANI*¹, T. GUENTHER*, C. LIENAU*, R. NÖTZEL† AND K. H. PLOOG†

*Max-Born-Institut für Nichtlineare Optik und Kurzzeitspektroskopie, D-12489 Berlin, Germany

†Paul-Drude-Institut für Festkörperelektronik, D-10117 Berlin, Germany

Key words. Carrier transport, femtosecond time resolution, near-field microscopy, pump-probe spectroscopy, quantum wire.

Summary

Quasi-two-colour femtosecond pump and probe spectroscopy and near-field scanning optical microscopy are combined to study the carrier dynamics in single semiconductor nanostructures. In temporally, spectrally and spatially resolved measurements with a time resolution of 200 fs and a spatial resolution of 200 nm, the non-linear change in reflectivity of a single quantum wire is mapped in real space and time. The experiments show that carrier relaxation into a single quantum wire occurs on a 100 fs time scale at room temperature. Evidence is given for a transient unipolar electron transport along the wire axis on a picosecond time and 100 nm length scale.

Introduction

Time-resolved optical spectroscopy, in particular with femtosecond resolution, has provided a wealth of information on dynamic processes such as the dephasing, scattering and energy relaxation of free carriers and excitons in semiconductor nanostructures and has led to a detailed understanding of these processes (Shah, 1999). Yet, the lack of sufficient, subwavelength spatial resolution often precludes direct insight into spatio-temporal dynamics of optical excitations in nanostructures. Specifically, real space transfer, trapping and relaxation processes of photogenerated carriers in low-dimensional semiconductors are of interest from the viewpoint of fundamental physics as well as device applications. Here, the combination of femtosecond spectroscopy with microscopy techniques giving submicron resolution, such as near-field scanning optical microscopy (NSOM) (Pohl *et al.*, 1984; Betzig & Trautman,

1992) offers new perspectives for a direct investigation of carrier dynamics on nanometre length scales. First experimental activities in this novel field of research have focused on combining ultrafast spectroscopy and near-field microscopy for studies of GaAs microdisks (Stark *et al.*, 1996) and quantum wells (Smith *et al.*, 1998), carrier diffusion in ion-implanted GaAs quantum wells (Achermann *et al.*, 1999; Nechay *et al.*, 1999) and exciton spin dynamics in magnetic heterostructures (Levy *et al.*, 1996). Recently, it was demonstrated that disorder-induced fluctuations of the excitonic resonance energy along the axis of a single QWR can be detected using near-field pump-probe spectroscopy (Achermann *et al.*, 2000).

In this paper, we combine near-field microscopy and femtosecond pump and probe spectroscopy to resolve the non-linear optical response from a single (311) GaAs quantum wire (QWR) structure in real space and time. We use this technique to investigate the carrier relaxation dynamics in a single QWR and to map the carrier transport dynamics along the QWR at room temperature.

Experimental

Quantum wires with a lateral width of 50 nm and a thickness of up to 13 nm embedded in a 6-nm GaAs quantum well (QW) were grown by molecular beam epitaxy on patterned GaAs (311)A substrates along the sidewalls of 15–20 nm high mesa stripes orientated along the $[0\bar{1}1]$ direction (Nötzel *et al.*, 1996). The QWR/QW layer is clad between two 50 nm thick $\text{Al}_{0.5}\text{Ga}_{0.5}\text{As}$ lower and upper barrier layers. The upper barrier is covered by a 20-nm thick GaAs cap layer. The total 1D confinement energy barrier of the QWR is about 80 meV (Fig. 1) (Richter *et al.*, 1997a; Lienau *et al.*, 1998). The pronounced 1D confinement results in a splitting of 10 meV between the lowest conduction band sub-bands. It gives rise to intense QWR photoluminescence (PL) at room temperature (centred around 1.46 eV), spectrally

Correspondence: T. Guenther. Tel: +49 30 6392 1472; fax: +49 30 6392 1489; e-mail: guenther@mbi-berlin.de

¹Present address: LENS, Laboratorio Europeo di Spettroscopie non-Lineari, I-50125 Firenze, Italy.

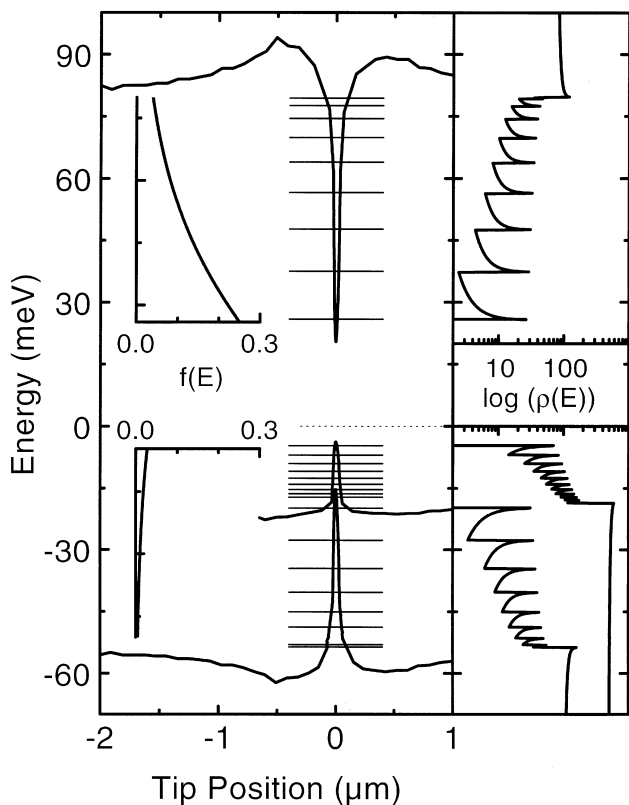


Fig. 1. Lateral confinement potential of the QWR structure, as derived from spatially resolved photoluminescence excitation spectroscopy. The horizontal lines indicate the calculated sub-band energies. The right graph shows the density of states $\rho(E)$ in the QWR and embedding QW region and the inset the electron and hole distribution functions $f(E)$ for localized excitation of a density of 10^{11} cm^{-2} electron-hole pairs in a 400-nm diameter spot.

well separated from the QW PL at 1.52 eV (Richter *et al.*, 1997b).

The experimental set-up that is used for spatially and temporally resolved pump-probe experiments is shown in Fig. 2. Both pump and probe pulses are derived from a mode-locked Ti:sapphire oscillator providing 20–40 fs pulses that are tunable in the wavelength range from 810 to 870 nm. The laser works at a repetition rate of 80 MHz and gives an average power of up to several hundreds of milliwatts. The laser output is split into a pump and a probe beam, each of which are travelling through a separate prism set-up for spectral selection and pre-compensation of group velocity dispersion (GVD) in the fibre. GVD in a fibre of length L transforms a bandwidth-limited Gaussian input pulse of duration τ_{in} into an output pulse of length $\tau_{\text{out}} = \tau_{\text{in}} \sqrt{1 + 4|k_d|^2 L^2 \tau_{\text{in}}^4}$ (Diels & Rudolph, 1996) where the GVD parameter $k_d = \partial^2 k / \partial \omega^2$, with k being the wavevector and ω the angular frequency. Higher order dispersion is neglected in this formula. For

quartz single mode fibres at laser wavelengths around 800 nm, $k_d \sim 100 \text{ ps}^2 \text{ km}^{-1}$.

In a 50-cm long fibre, a 50 fs input pulse is thus stretched to an about 2 ps long chirped pulse. For such fibre lengths, pulse widths of about 100 fs are routinely obtained with standard prism compressors, whereas third-order dispersion should also be compensated to reach shorter pulse lengths. Pump and probe beams are mechanically chopped at frequencies $f_1 \approx 1.2 \text{ kHz}$ and $f_2 = 1.77 f_1$, respectively. Two different optical configurations are used (Fig. 3). In a far-field pump/near-field probe geometry (FFNF), only the probe pulse is sent through the near-field fibre probe, while the pump is focused through a far-field lens to a spot size of about $30 \mu\text{m}$. In a near-field pump/near-field probe geometry (NFNF), both pump and probe pulses are transmitted through the same near-field tip, resulting in overlapping subwavelength excitation and probe spots. The time delay between pump and probe is adjusted with a delay stage in the pump arm. After interaction with the sample, the transmitted or reflected probe light is collected through standard long working-distance microscope objectives and detected by a photodiode in conjunction with a lock-in amplifier. For suppression of background signals, the lock-in amplifier detects the amplified photodiode signal at the sum frequency, $f_1 + f_2$. Near-field fibre probes are made by chemically etching single mode optical fibres to a sharp taper (Lambelet *et al.*, 1998). In the experiments, these fibres were used without metal coating. All data were taken at a sample temperature of 300 K.

Non-linear optical response of a single quantum wire

A first set of experiments was performed at a fixed delay time $t_d = 10 \text{ ps}$ between pump and probe pulses in order to spectroscopically assign the non-linear optical response of a single quantum wire.

First, far-field pump/near-field probe spectra were recorded in the QW region of the sample. The pump pulses with a bandwidth 40 meV are centred around the QW absorption resonance at 1.52 eV. The excitation density was about $3 \times 10^{11} \text{ cm}^{-2}$. The pump-induced change in reflectivity was measured with tunable probe pulses of 11 meV bandwidth. In Fig. 4 (○), the reflectivity change $\Delta R/R_0(t_d) = (R(t_d) - R_0)/R_0$ for a time delay t_d of 10 ps between pump and probe is plotted as a function of E_{pr} (R, R_0 : sample reflectivity with and without pump). The spectrum was recorded at a fixed tip position in the QW region of the sample. For photon energies E_{pr} of the probe between 1.51 eV and 1.55 eV, the creation of electron-hole pairs results in an increase in reflectivity. This spectrum shows a pronounced maximum at $E_{\text{pr}} = 1.515 \text{ eV}$ and follows – for $E_{\text{pr}} \geq 1.515 \text{ eV}$ – the shape of the QW photoluminescence excitation spectrum. In contrast, for $E_{\text{pr}} < 1.51 \text{ eV}$, we find a decrease in reflectivity. For

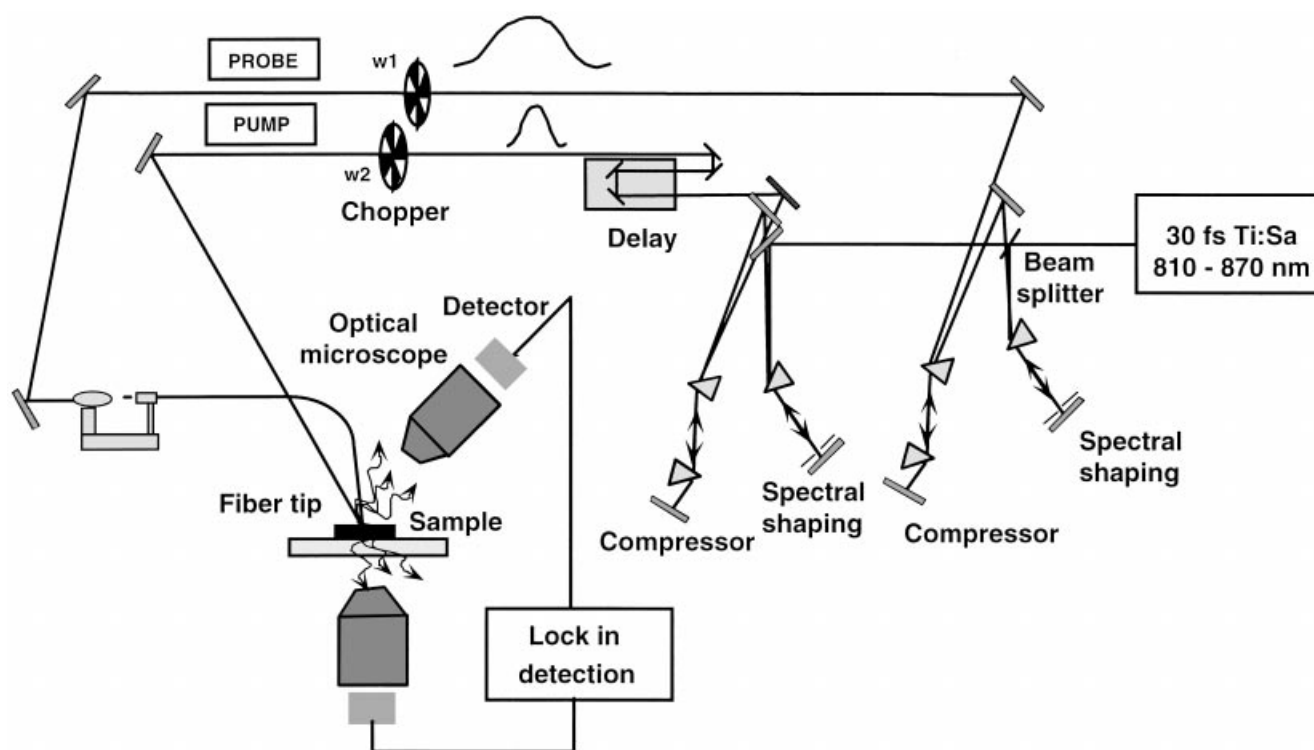


Fig. 2. Schematic of the experimental set-up for femtosecond near-field spectroscopy. Pump and probe pulses are derived from a mode-locked Ti:sapphire laser using two independent arrangements for spectral shaping and compression. In the far-field pump/near-field probe configuration shown, the pump excites a large area of the sample. The probe laser is fed into a near-field probe, allowing for a spatially resolved detection of ultrafast transmission or reflection changes. The non-linear changes of transmission or reflection are measured with the help of a lock-in technique.

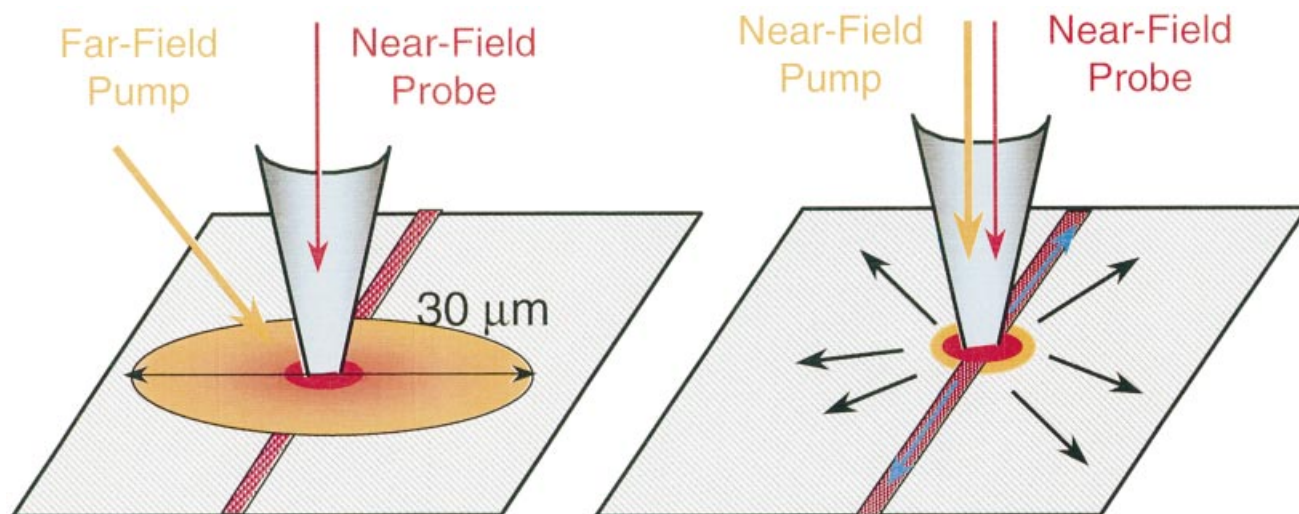


Fig. 3. Two different experimental configurations are used. In a far-field pump/near-field probe geometry electron-hole pairs are generated in a 30- μm spot by focusing the pump laser with a far-field lens. The carrier-induced modulation of the sample reflectivity is locally probed with a near-field fibre probe. In a near-field pump/near-field probe geometry electron-hole pairs are locally created and reflectivity changes are locally probed by transmitting both pump and probe pulses through the same near-field fibre probe. This allows us to study the carrier transport dynamics along the wire axis.

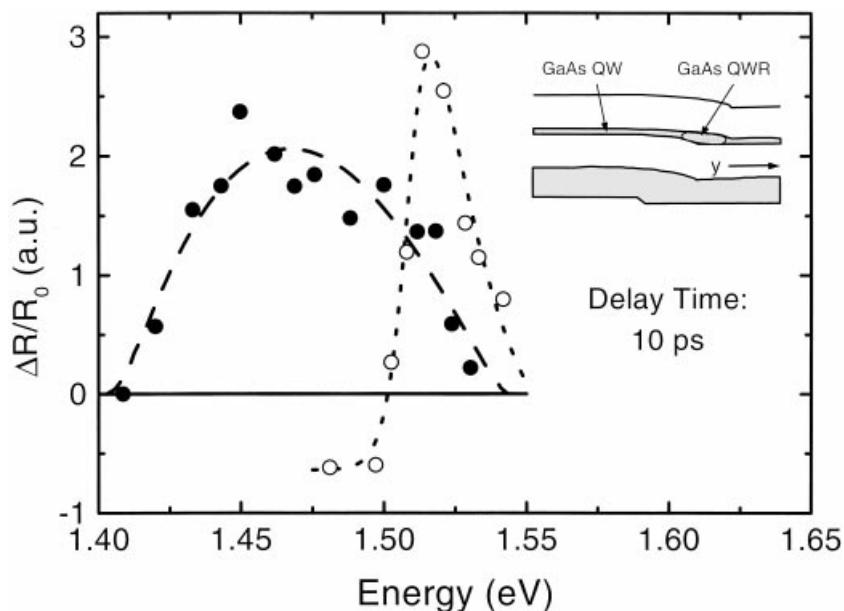


Fig. 4. Probe wavelength dependence of $\Delta R_{\text{QWR}}(t_d = 10 \text{ ps})/R_0$ (●) and of the reflectivity change in the mesa top region of the sample (○). $\omega_{\text{pu}} = 1.52 \text{ eV}$. Inset: Schematic of the sidewall quantum wire structure.

excitation densities between 10^{10} and $3 \times 10^{11} \text{ cm}^{-2}$, the magnitude of $\Delta R/R_0$ is proportional to the pump intensity.

Next, we present data taken for probe energies in the range of the QWR resonance around 1.46 eV. In this measurement, both pump and probe were transmitted through the fibre probe. Excitation at 1.48 eV generates carriers exclusively in the QWR which give rise to a local change of reflectivity. This is evident from the image in Fig. 5(a) where the change of reflectivity at $E_{\text{pr}} = 1.45 \text{ eV}$ and a delay time of 10 ps is plotted as a function of two spatial coordinates in the QW plane. The pronounced local change of reflectivity occurs along a line that coincides with the QWR position at the sidewall of the $[0\bar{1}1]$ mesa stripes. This position is independently identified from simultaneously recorded shear-force topography images. The local reflectivity change is superimposed on a spatially slowly varying background signal which is due to the GaAs cap and substrate layers. In Fig. 5(b) (●), the quantity $\Delta R(y)/R_0$ is plotted along the y direction, i.e. perpendicular to the QWR axis ($y = 0$: QWR position). The local reflectivity peak is measured with a spatial resolution of 200 nm. The variation of the reflectivity change $\Delta R_{\text{QWR}}/R_0 = (\Delta R(y = 0) - \Delta R(|y| > 1 \mu\text{m}))/R_0$ with probe energy E_{pr} is presented in Fig. 4 (●) for a delay of 10 ps ($\Delta R(|y| > 1 \mu\text{m})$: background signal). The line-shape resembles the shape of the room temperature PLE spectrum (Richter *et al.*, 1997b). For excitation at a lower photon energy of 1.44 eV where the QWR absorption is negligible, the reflectivity change $\Delta R_{\text{QWR}}/R_0$ vanishes completely (Fig. 5b, ○).

To interpret these experiments we performed an analysis of the local carrier-density dependent reflectivity spectra of

our sample. For multilayer semiconductor nanostructures, such spectra depend sensitively on the details of the layer sequence. Their interpretation thus requires an analysis of the probe pulse propagation through the multilayer nanostructure which in our case consists of the GaAs cap layer, the GaAs QW in which the QWR is embedded, the GaAs substrate and, in-between, the AlGaAs barriers. The generation of carriers by the pump pulse leads to a modification of the optical susceptibility $\chi(\omega, n_{\text{ex}})$ of each layer with carrier density n_{ex} . This results in a change of reflectivity measured at the different probe wavelengths. A numerical simulation of these changes assuming thermalized carrier distributions for both electrons and holes was performed by using the numerical matrix inversion method (Schmitt-Rink *et al.*, 1986). The assumption of thermalized distributions is reasonably justified, as our time resolution is less than the sub100 fs dephasing and thermalization times of free carriers in 2D quantum wells at room temperature (Knox *et al.*, 1988; Bigot *et al.*, 1991; Kim *et al.*, 1992). The model accounts quantitatively for the influence of phase-space filling, screened Coulomb interaction, here treated in a static approximation, and band-gap renormalization on $\chi(\omega, n_{\text{ex}})$. It gives absolute values for the density dependent absorption coefficient $\alpha(\omega, n_{\text{ex}})$ and refractive index $n_{\text{r}}(\omega, n_{\text{ex}})$ of each layer. A transfer matrix formalism is then used to derive the reflectivity $R(\omega, n_{\text{ex}})$ and the carrier-induced change in reflectivity $\Delta R(\omega, n_{\text{ex}}) = R(\omega, n_{\text{ex}}) - R(\omega, 0)$ for the multilayer structure.

The results of these simulations are summarized in Fig. 6 and suggest the following interpretation (Guenther *et al.*, 1999). Excitation of the QW ($E_{\text{pump}} > 1.5 \text{ eV}$) gives rise to a

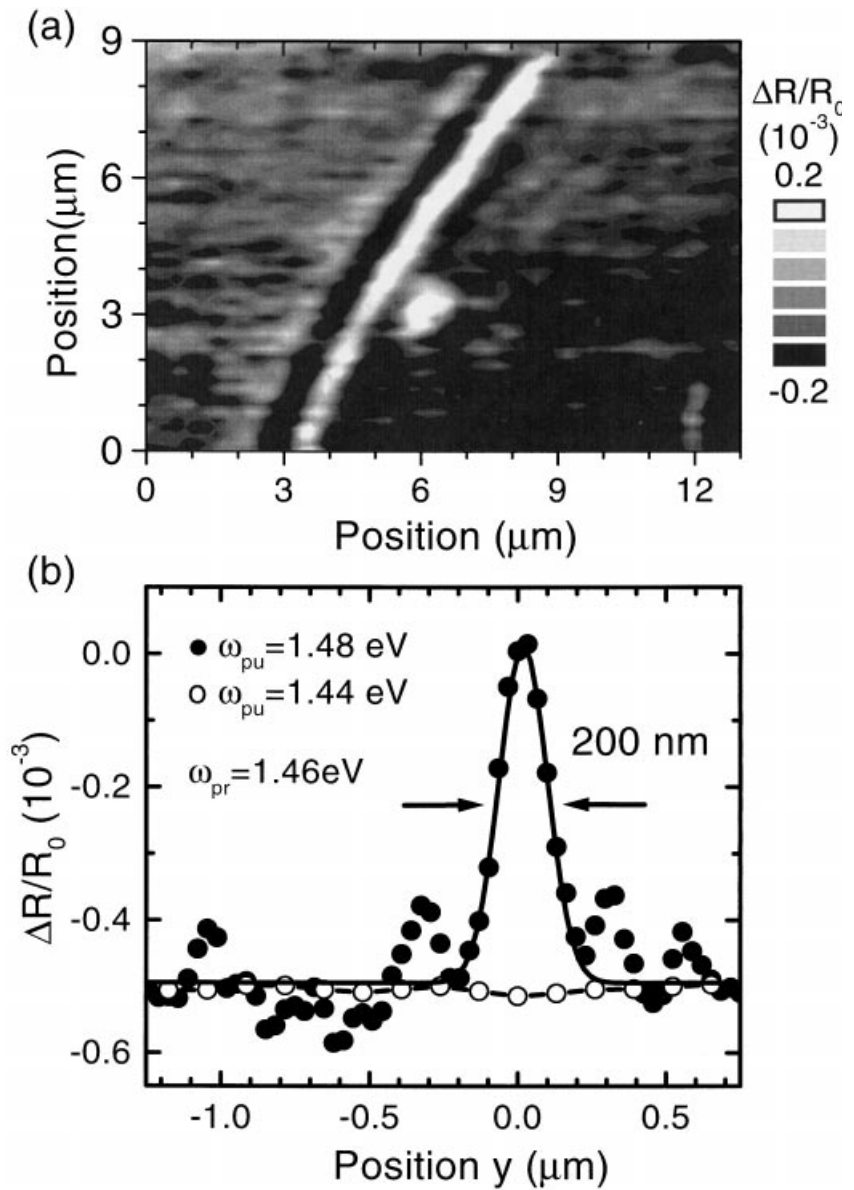


Fig. 5. (a) Spatial map of the pump-induced reflectivity change $\Delta R/R_0$ at a delay time t_d of 10 ps. The probe laser is set to 1.45 eV, i.e. resonant to the excitonic QWR absorption peak at room temperature. (b) Spatial variation of $\Delta R/R_0$ along a line perpendicular to the wire axis at a probe wavelength of $E_{pr} = 1.46$ eV. \bullet : $E_{pu} = 1.48$ eV, i.e. resonant QWR excitation. \circ : $E_{pu} = 1.44$ eV, i.e. excitation below the excitonic QWR absorption. Note that the local change in reflectivity vanishes completely for excitation at $E_{pu} = 1.44$ eV.

pronounced bleaching of the excitonic QW absorption resonance at $E_{pr} = 1.52$ eV, i.e. of the imaginary part of the susceptibility. This results in an increase in reflectivity with a spectral dependence close to the QW PLE spectrum. Carriers in the GaAs cap and substrate layers also give rise to a bleaching of the absorption around the band gap of each layer. Yet, here the reflectivity changes are of an opposite sign, i.e. the simulations predict a decrease in reflectivity for probe energies $E_{pr} < 1.5$ eV. The change in sign occurs because of the large jump in refractive index at the cap layer/air interface. This makes the carrier-density dependent reflectivity change most sensitive to the change in refractive index in the GaAs cap layer, i.e. the real part of

the susceptibility. The experimentally measured reflectivity changes (Fig. 4, \circ) consist of the sum of the contributions from QW and cap layer and therefore show an increase in reflectivity for $E_{pr} > 1.51$ eV (QW contribution dominant) and a decrease in reflectivity for $E_{pr} < 1.51$ eV (cap layer contribution dominant). For the QWR, the simulations predict, as for the QW, a bleaching of the excitonic QWR absorption and a corresponding increase in reflectivity with a spectral dependence that follows the QWR PLE spectrum, similar to the experimentally observed spectra shown in Fig. 4 (\bullet). The QWR reflectivity change is again superimposed on the negative background from the cap layer change in reflectivity. For a spatial resolution of the probe

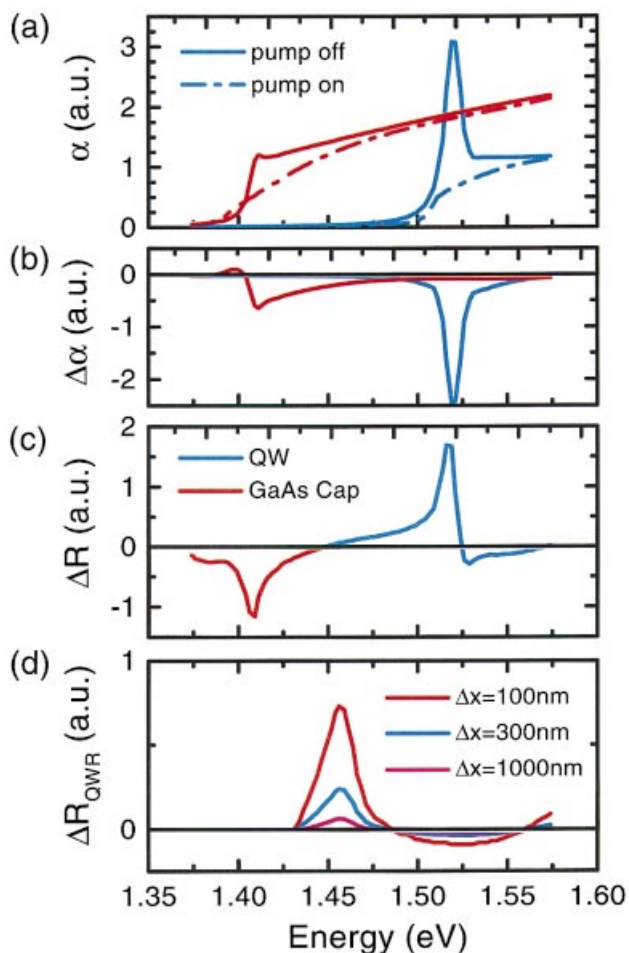


Fig. 6. (a) Absorption spectra of bulk GaAs (red lines) and a 6-nm GaAs quantum well (blue lines) simulated using the numerical matrix inversion method as a function of the optically excited carrier density n_{ex} . Shown are spectra for $n_{ex,off} = 0$ (solid line, pump off) and for $n_{ex,on} = 10^{11} \text{ cm}^{-2}$ (dashed line, pump on) assuming thermalized distributions of electron-hole pairs at room temperature. (b) Carrier-induced change in absorption coefficient $\Delta\alpha = \alpha(n_{ex,on}) - \alpha(n_{ex,off})$. (c) Carrier-induced change in reflectivity $\Delta R = R(n_{ex,on}) - R(n_{ex,off})$ calculated for the bulk GaAs cap layer the 6 nm GaAs QW using a transfer matrix formalism for the multilayer structure shown schematically in Fig. 4. (d) Carrier-induced change in QWR reflectivity $\Delta R(QWR) = R(n_{ex,on}) - R(n_{ex,off})$ calculated using the numerical matrix inversion and transfer matrix formalism for the multilayer structure shown schematically in Fig. 4. As the QWR width of 50 nm is smaller than the optical resolution, the magnitude of $\Delta R(QWR)$ depends approximately linearly on the spatial resolution Δx of the probe spot.

beam that is less than the lateral width of the QWR of 50 nm, the magnitude of the reflectivity change from a single QWR will decrease roughly linearly with decreasing spatial resolution, making it very difficult to resolve the QWR signal with far-field resolution.

Finally, we would like to comment on the optical resolution in our experiments. The data presented in Fig. 5(b) show that

the QWR reflectivity change $\Delta R_{QWR}/R_0$ is recorded with a spatial resolution of 200 nm. These experiments were performed with uncoated fibre probes with a taper angle of 30° . A theoretical analysis of the propagation of femtosecond pulses through such uncoated fibre probes predicts indeed a diffraction limited resolution of about 260 nm at the exit of the fibre probe (Müller & Lienau, 2000). In pump-probe experiments where both pump and probe pulse are transmitted through the same fibre, the resolution should be improved even further. A resolution of less than 200 nm is expected, in agreement with the experimental finding and the results reported by Lewis *et al.* (1998).

Carrier relaxation and transport in a single quantum wire

In this section we analyse the carrier dynamics in the QWR by studying the temporal variation of $\Delta R_{QWR}(t_d)$ for different excitation conditions. First, experiments performed with far-field excitation (FFNF) are presented (Fig. 7). Here, carriers are generated with a 50 fs far-field pulse with a spot size of 30 μm . The pump laser is centred at 1.52 eV in order to overlap the absorption spectrum of the QW. At this energy, a spatially homogeneous carrier distribution is generated in high-energy QWR states, in the embedding QW and in the GaAs cap and substrate layers. The density generated by the pump pulse was 10^{11} cm^{-2} , corresponding to non-degenerate excitation conditions ($T = 300 \text{ K}$). Probe pulses at 1.46 eV, near the QWR resonance, were transmitted through the fibre probe. On both sides of the QWR (Fig. 7a), a spatially homogeneous transient reflectivity decrease is observed that decays on a time scale of several ps (Fig. 7b and 8a, ●). This signal is dominated by the transient carrier-induced reflectivity change of the GaAs cap layer and the picosecond decay of the change in reflectivity reflects the trapping of carriers into surface states (Baumberg *et al.*, 1997).

In contrast, an initial decrease in reflectivity with a smaller amplitude and an increase in reflectivity for delay times longer than 5 ps occurs at the QWR position, $y = 0$ (Fig. 7b and 8a, ○). The QWR contribution, ΔR_{QWR} , is extracted by taking the difference of the two transients in Fig. 7(b) and 8(a), respectively. On an early time scale, the temporal evolution of ΔR_{QWR} (Fig. 8b) shows a step-like behaviour with an ultrafast rise within 200 fs, the time resolution of the experiment. The value of ΔR_{QWR} remains constant up to delay times of 50 ps (Fig. 7c). A similar temporal evolution of ΔR_{QWR} is observed for resonant far-field excitation of the QWR ($E_{pu} = 1.47 \text{ eV}$) and spatially resolved probing at energies of high-lying QWR states around 1.51 eV (Fig. 9).

Different dynamics are observed when both pump and probe pulses are transmitted through the near-field fibre probe (NFNF), as shown in Fig. 10. The spectra of the pump

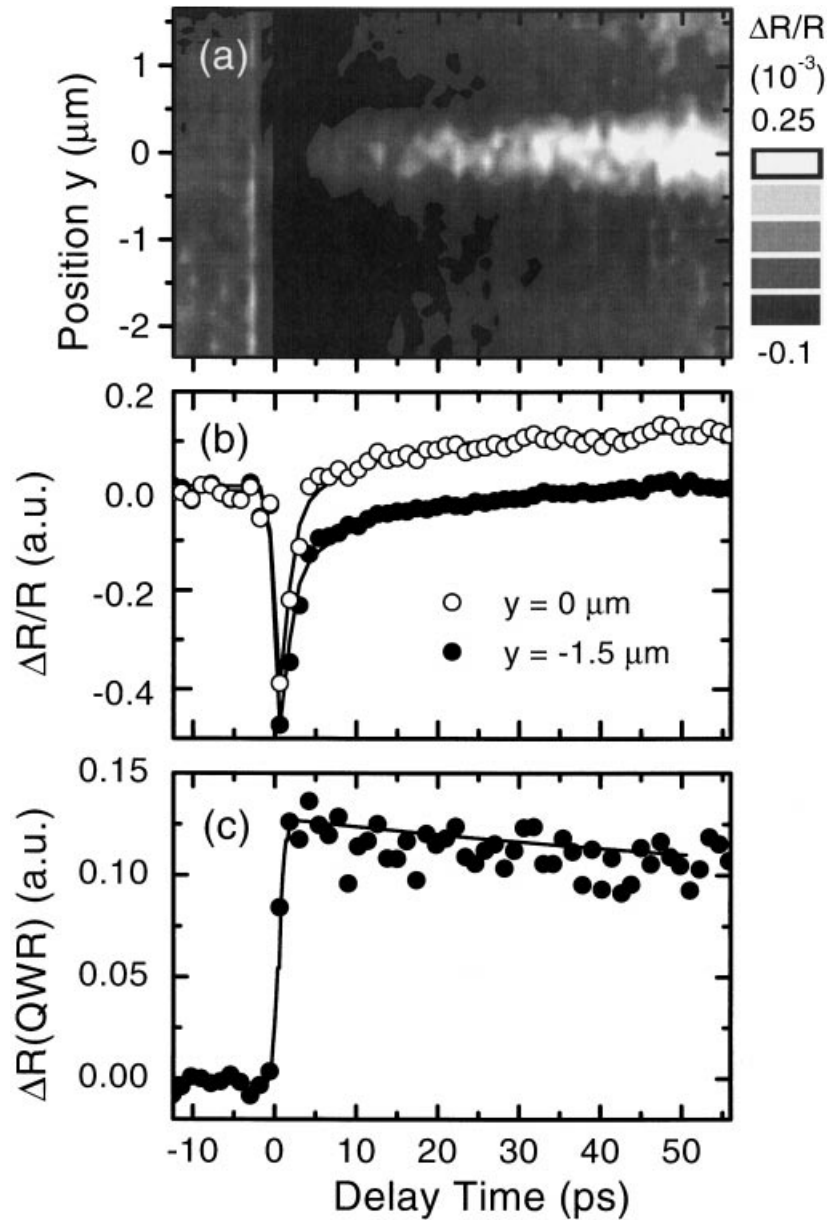


Fig. 7. (a) Pump-induced reflectivity change $\Delta R/R$ as a function of tip position along the y -axis, perpendicular to the QWR, and as a function of delay time t_d on a time scale of up to 50 ps. The excitation is performed with a far-field spot having a diameter of 30 μm (FFNF). The pump laser is centred at $E_{\text{pu}} = 1.52$ eV to create electron–hole pairs in high-lying QWR states and in the embedding QW. The probe laser at $E_{\text{pr}} = 1.46$ eV probes the local bleaching of the excitonic QWR absorption. (b) Temporal variation of $\Delta R/R$ at fixed spatial probe positions of $y = 0$ (QWR position, \circ) and on the mesa top part at $y = 1.5$ μm . (c) $\Delta R_{\text{QWR}}(t_d)/R_0 = (\Delta R(y = 0, t_d) - \Delta R(y = 1.5 \mu\text{m}, t_d))/R_0$.

and probe lasers are shown in the inset of Fig. 10(b). For tip positions outside the QWR region, we observe again, as for far-field excitation, a spatially homogeneous transient reflectivity decrease that decays on a time scale of few ps. This signal reflects again the trapping of carriers in the cap layer into surface states. As described above, we extract $\Delta R_{\text{QWR}}(t_d)$ by taking the difference in the transients recorded at the QWR position, $y = 0$, and for tip positions $|y| > 1$ μm . For near-field excitation, the transient of $\Delta R_{\text{QWR}}(t_d)$ shown in Fig. 10(b) now reveals a clear decay by more than 50% on a time scale of 50 ps – in contrast to the time-independent reflectivity change for far-field excitation. Similar spatio-temporal maps of the local reflectivity

changes for near-field excitation are recorded when the probe energy is varied between 1.43 eV and 1.5 eV. Figure 11(a) shows spatio-temporal maps of the pump-induced reflectivity change $\Delta R(t_d, y)$ for three different probe energies. For each probe energy, $\Delta R_{\text{QWR}}(t_d)$ reveals a similar decay by about 30% within the first 20 ps. From a series of such measurements, we extracted transient spectra $\Delta R_{\text{QWR}}(E_{\text{pr}}, t_d)$ of the QWR reflectivity change (Fig. 12). At each delay time t_d , we observe a similar spectral dependence as in the room temperature QWR PLE spectrum (Richter *et al.*, 1997b). In particular, we find no indication for a time-dependent shift of $\Delta R_{\text{QWR}}(E_{\text{pr}}, t_d)$.

As discussed in the last section, the pump-induced

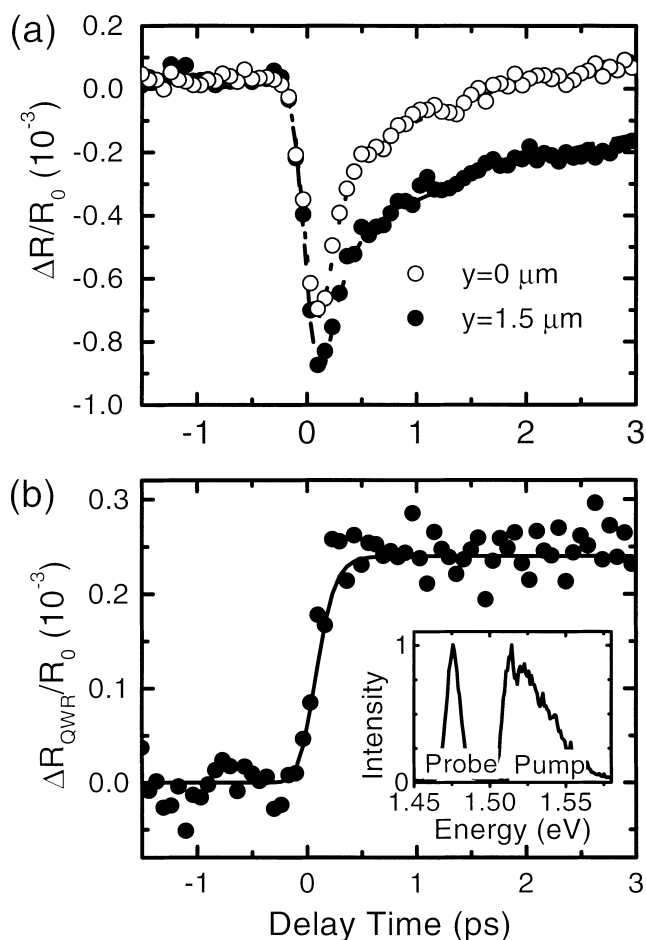


Fig. 8. (a) As Fig. 7(b) for delay times t_d between -1.5 and 3 ps. (b) Ultrafast rise of the carrier-induced change in QWR reflectivity $\Delta R_{\text{QWR}}(t_d)/R_0 = (\Delta R(y = 0, t_d) - \Delta R(y = 1.5 \mu\text{m}, t_d))/R_0$. Inset: Spectra of pump and probe lasers centred at 1.52 eV and 1.46 eV, respectively.

change in the probe laser reflectivity, $\Delta R_{\text{QWR}}(t_d)$, arises from the carrier-induced bleaching of the excitonic QWR absorption. This bleaching is due to photoexcited carriers inside the QWR and thus $\Delta R_{\text{QWR}}(t_d)$ is an efficient probe for the temporal evolution of the QWR carrier density. In quantum wells at room temperature and for carrier densities that are similar to those in our experiments, phase-space filling, i.e. the occupation of the single particle states that contribute to bound exciton states, gives the main contribution to the bleaching of the excitonic absorption (Hunsche *et al.*, 1994). It causes a direct reduction of the excitonic oscillator strength and gives rise to a spectral dependence of ΔR_{QWR} that is similar to the excitonic absorption spectrum. We expect that phase-space filling also dominates the bleaching of the excitonic QWR absorption and thus ΔR_{QWR} . The

phase-space filling and therefore also the magnitude of the bleaching of the excitonic QWR absorption and of ΔR_{QWR} are sensitive probes of the local concentrations of electrons and holes within the QWR region. The observation of a reflectivity change for probe energies around 1.46 eV thus requires carrier redistribution from optically excited high lying QWR to low energy states at the bottom of the QWR. The absence of any slower dynamics on the transient in Fig. 8(b) suggests that this redistribution process occurs within the first 200 fs. At room temperature and under our excitation conditions this relaxation involves a complex scattering scenario with contributions from both carrier-LO phonon scattering (typical phonon emission times in QWRs are about 150 fs) and carrier-carrier scattering. The ultrafast rise in reflectivity that is observed when the pump is tuned in resonance with the QWR absorption and the probe wavelength is set to high-lying QWR states (Fig. 9) suggests that a thermalized carrier distribution is formed within the first 200 fs, similar to the thermalization dynamics in quantum wells. This conclusion is supported by the time-independent shape of the transient spectra $\Delta R_{\text{QWR}}(E_{\text{pr}}, t_d)$ shown in Fig. 12.

In the experiments performed with far-field excitation, i.e. with an excitation spot of $30 \mu\text{m}$ diameter, a homogeneous carrier distribution is generated. Thus, the diffusive ambipolar motion of carriers within the embedding QW (for which a RT diffusion coefficient of $D_{\text{QW}} = 12 \text{ cm}^2 \text{ s}^{-1}$ was measured in our sample) (Richter *et al.*, 1997a) does not significantly enhance the QWR carrier density on a ps time scale. Therefore the reflectivity signal remains roughly constant within the first 50 ps (Fig. 7b). It is likely to decay with the electron-hole recombination time of 1.9 ns,

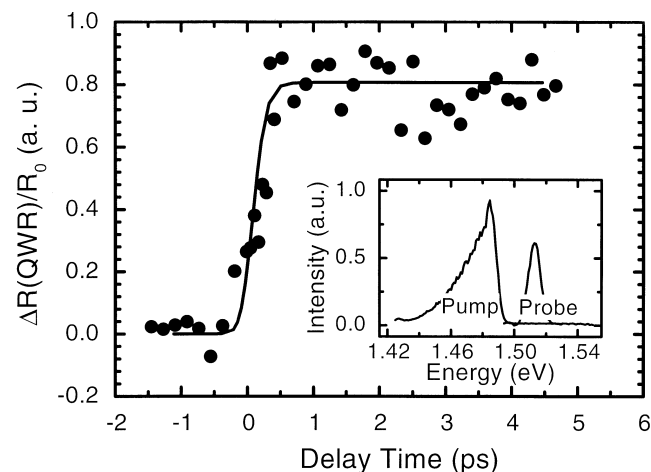


Fig. 9. Carrier-induced change in QWR reflectivity $\Delta R_{\text{QWR}}(t_d)/R_0 = (\Delta R(y = 0, t_d) - \Delta R(y = 1.5 \mu\text{m}, t_d))/R_0$ for resonant QWR excitation at 1.47 eV and probing at 1.52 eV. Inset: Spectra of pump and probe lasers.

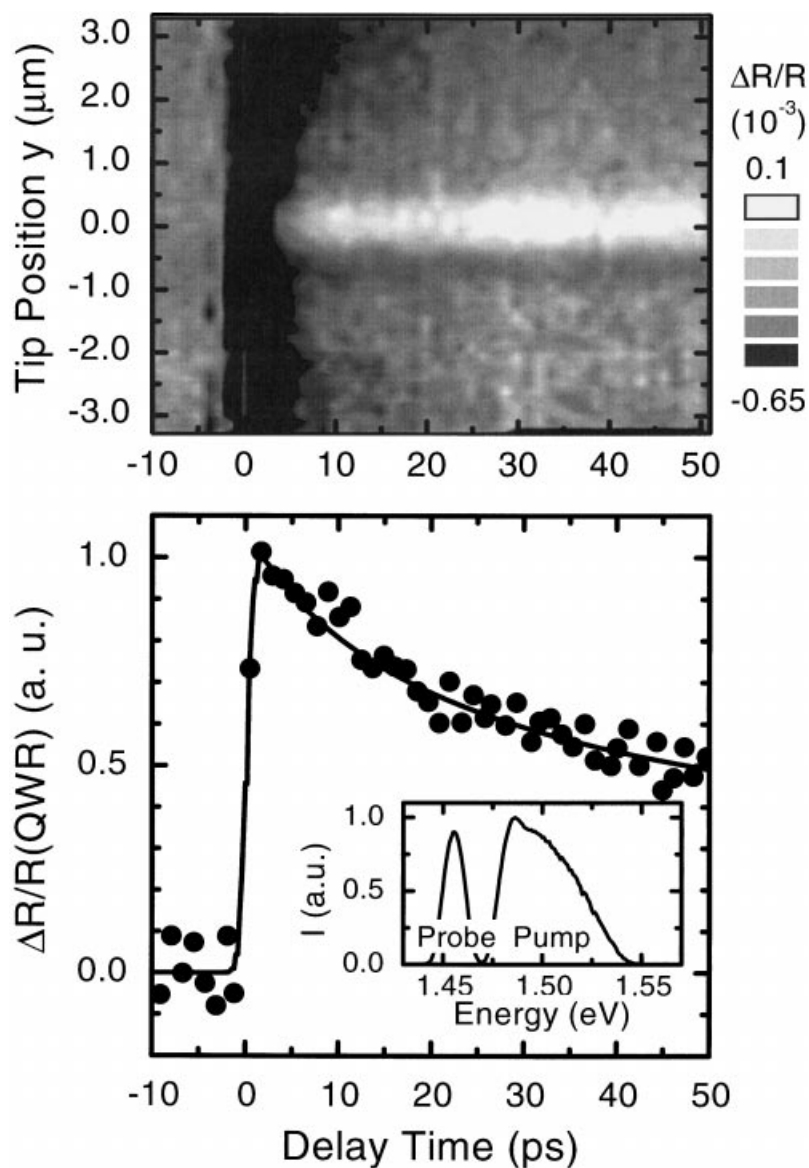


Fig. 10. (a) Pump-induced reflectivity change $\Delta R/R_0$ as a function of tip position along the y -axis, perpendicular to the QWR, and as a function of delay time t_d on a time scale of up to 50 ps. The excitation is performed with a spatial resolution of less than 400 nm (NFNF) by transmitting the pump pulses through the same fibre probe as the probe pulses. (b) Temporal variation of the pump-induced reflectivity change $\Delta R(QWR)/R_0$ at the QWR position. The decay of the reflectivity signal reflects the carrier transport along the QWR. The solid line shows a simulation of a 1D diffusion model with $D_{QWR} = 80 \text{ cm}^2 \text{ s}^{-1}$. Inset: Spectra of pump and probe lasers, centred at 1.50 and 1.46 eV, respectively.

identical to the QWR luminescence decay time at room temperature (Richter *et al.*, 1997a).

For near-field excitation we observe, on the contrary, a clear decay of $\Delta R_{QWR}(t_d)$ on a 10-ps time scale. Here, both the excitation and probe pulses, spatially overlapping, are localized to a small spot of about 400 nm in diameter. Therefore the optically injected carriers migrate out of the excitation volume on a ps time scale. This results in a decrease of the local carrier concentration and thus in a reduction of ΔR_{QWR} . In general, the transport of carriers out of the excited volume can occur both along the QWR as well as perpendicular to it. The data in Figs 8 and 12 suggest that quasi-equilibrium Fermi distributions in both QWR and QW states are formed within 200 fs. The density of states

$\rho(E)$ and distribution functions $f(E)$ for electrons and holes in such a non-degenerate distribution with a carrier density of 10^{11} cm^{-2} are schematically depicted in Fig. 1. Due to the difference in confinement potentials for electrons (65 meV) and heavy holes (15 meV) the spatial distributions of electrons and holes are strongly different in such a thermalized distribution. The density of electrons in the QWR is estimated to be about four times higher than the QWR hole density. This means that a large fraction of the photoexcited electrons is confined inside the QWR whereas most of the holes are populating quasi-continuum states of the embedding QW. Thus $\Delta R_{QWR}(t_d)$ probes mainly the local dynamics of electrons inside the QWR. Considering the small fraction of electrons that is

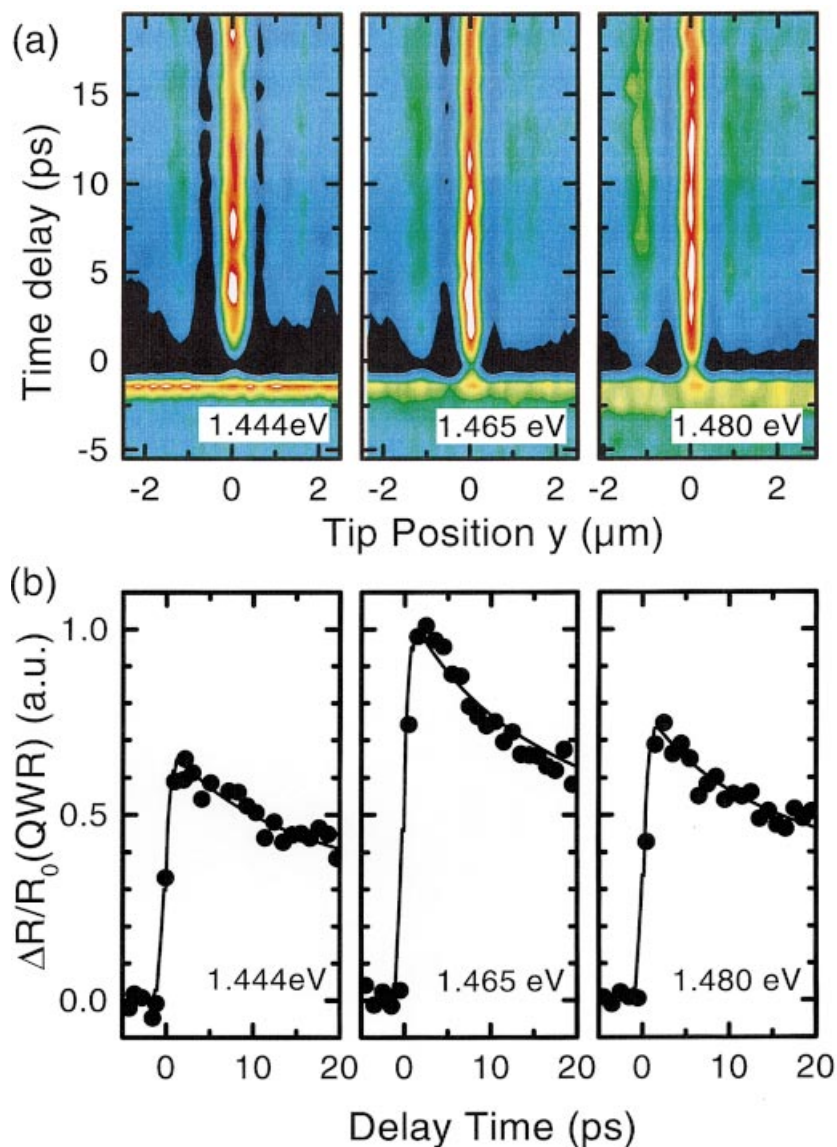


Fig. 11. (a) Probe-wavelength dependence of the pump-induced reflectivity change $\Delta R/R_0$ recorded as a function of tip position along the y -axis, perpendicular to the QWR, and as a function of delay time t_d on a time scale of up to 20 ps. The experiments are performed with localized near-field excitation with a spatial resolution of less than 400 nm. (b) Time dependence of $\Delta R(QWR)/R_0$ for probe lasers centred at 1.444, 1.467 and 1.478 eV, respectively. Excitation conditions as in Fig. 10.

populating QW continuum states and the ambipolar QW diffusion coefficient $D_{QW} = 12 \text{ cm}^2 \text{ s}^{-1}$, one finds a negligible contribution of the lateral transport, perpendicular to the QWR axis, to the transients in Figs 10(b) and 11(b). We can therefore conclude that the decay of the reflectivity transients reflects mainly the transport dynamics of electrons along the QWR.

Assuming that the transport along the QWR – on a time scale of several picoseconds – is adequately represented within a 1D-diffusion model, the experimental curves can be simulated, having the diffusivity as the only unknown parameter (Emiliani *et al.*, 2000). The observed decay of the QWR reflectivity is well described by taking a quasi-one-dimensional diffusion coefficient $D_{QWR} = 80 \pm 20 \text{ cm}^2 \text{ s}^{-1}$ (solid line in Fig. 10b). This value of the 1D diffusion

coefficient is surprisingly high. In fact it is more than five times larger than the ambipolar 2D diffusion coefficient $D_{QW} = 12 \text{ cm}^2 \text{ s}^{-1}$ measured in the QW area of the sample. The 2D value, using the Einstein relation $\mu = eD/k_B T$ (e : electron charge, $k_B T$: thermal energy), corresponds to a mobility of $\mu_{QW} = 500 \text{ cm}^2 \text{ Vs}^{-1}$, which is close to the mobility of holes in GaAs at 300 K. In this case, hole diffusion limits the ambipolar transport through the QW Richter *et al.*, 1997a). On the contrary, the diffusion coefficient $D_{QWR} = 80 \pm 20 \text{ cm}^2 \text{ s}^{-1}$ corresponds to a mobility $\mu_{QWR} = 3000 \text{ cm}^2 \text{ Vs}^{-1}$ which is close to the RT mobility of electrons in GaAs. This suggests that, in our experiments, the transport of electrons along the QWR axis is strongly different from a conventional ambipolar diffusive transport regime, with a spatially and temporally correlated

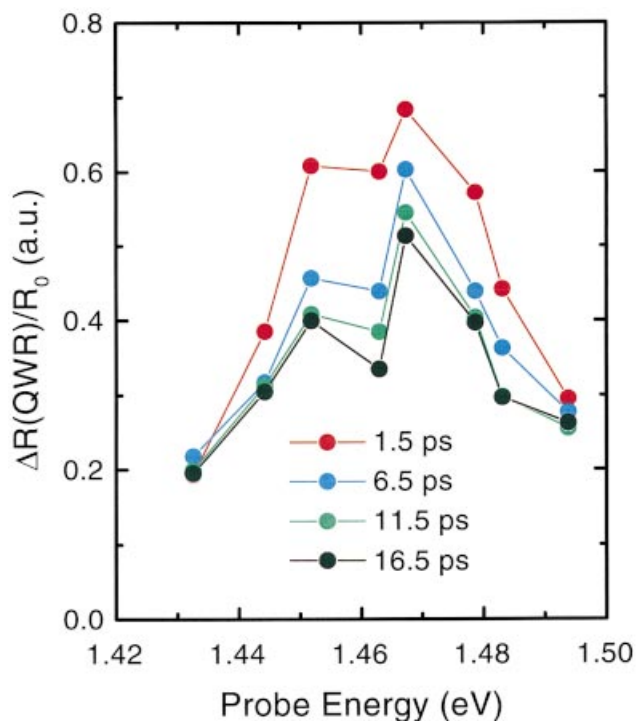


Fig. 12. Spectral dependence of the pump-induced QWR reflectivity change $\Delta R_{\text{QWR}}/R_0(E_{\text{pr}}, t_d)$ for fixed delay times between 1.5 and 16.5 ps.

motion of electrons and holes and a mobility that is hole-limited. Instead we are observing a rapid motion of electrons out of the excitation volume, along the QWR axis. The experiments suggest a unipolar transport of electrons along the wire axis as discussed by Emiliani *et al.* (2000). Experiments at cryogenic temperatures will help to unequivocally resolve the microscopic origin of the observed fast transport dynamics.

Conclusion

In conclusion, we have demonstrated the potential of femtosecond near-field spectroscopy for directly imaging the carrier dynamics in a single semiconductor nanostructure. Femtosecond pump-probe experiments with a near-field microscope demonstrate carrier trapping into the quantum wire on a 200 fs time scale at room temperature. Both Coulomb and optical phonon scattering of carriers contribute to this fast local relaxation. First pump-probe studies of carrier transport along the quantum wire suggest an electron mobility which is substantially higher than expected for conventional ambipolar diffusion of electron-hole pairs. The results indicate a unipolar transport of electrons along the wire axis. These experiments demonstrate the potential of femtosecond near-field techniques as

powerful novel tools for studying non-equilibrium carrier dynamics on ultrafast time and nanometre length scales.

Acknowledgements

This work has been supported by the Deutsche Forschungsgemeinschaft (SFB296) and the European Union through the Ultrafast Quantum Optoelectronics Network, the EFRE program and a Marie-Curie Fellowship (ERB4001GT975127) for one of the authors (V.E.).

References

- Achermann, M., Nechay, B.A., Morier-Genoud, F., Schertel, A., Siegner, U. & Keller, U. (1999) Direct experimental observation of different diffusive transport regimes in semiconductor nanostructures. *Phys. Rev. B* **60**, 2101–2105.
- Achermann, M., Nechay, B.A., Siegner, U., Hartmann, A., Oberli, D., Kapon, E. & Keller, U. (2000) Quantization energy mapping of single V-groove GaAs quantum wires by femtosecond near-field optics. *Appl. Phys. Lett.* **76**, 2695–2697.
- Baumberg, J.J., Williams, D.A. & Köhler, K. (1997) Ultrafast acoustic phonon ballistics in semiconductor heterostructures. *Phys. Rev. Lett.* **78**, 3358–3361.
- Betzig, E. & Trautman, J.K. (1992) Near-field optics: microscopy, spectroscopy, and surface modification beyond the diffraction limit. *Science* **257**, 189–193.
- Bigot, J.-Y., Portella, M.T., Schoenlein, R.W., Cunningham, J.E. & Shank, C.V. (1991) Two-dimensional carrier-carrier screening in a quantum well. *Phys. Rev. Lett.* **67**, 636–639.
- Diels, J.-C. & Rudolph, W. (1996) *Ultrashort Laser Pulse Phenomena*. Academic Press, San Diego.
- Emiliani, V., Guenther, T., Lienau, C., Nötzel, R. & Ploog, K.H. (2000) Ultrafast near-field spectroscopy of quasi-one-dimensional transport in a single quantum wire. *Phys. Rev. B* **61**, R10583–R10586.
- Guenther, T., Emiliani, V., Intonti, F., Lienau, C., Elsaesser, T., Nötzel, R. & Ploog, K.H. (1999) Femtosecond near-field spectroscopy of a single GaAs quantum wire. *Appl. Phys. Lett.* **75**, 3500–3502.
- Hunsche, S., Leo, K., Kurz, H. & Köhler, K. (1994) Exciton absorption saturation by phase-space filling: influence of carrier temperature and density. *Phys. Rev. B* **49**, 16565–16568.
- Kim, D.S., Shah, J., Cunningham, J.E., Damen, T.C., Schäfer, W., Hartmann, M. & Schmitt-Rink, S. (1992) Giant excitonic resonance in time-resolved four-wave mixing in quantum wells. *Phys. Rev. Lett.* **68**, 1006–1009.
- Knox, W.H., Chemla, D.S., Livescu, G., Cunningham, J.E. & Henry, J.E. (1988) Femtosecond carrier thermalization in dense Fermi seas. *Phys. Rev. Lett.* **61**, 1290–1293.
- Lambelet, P., Sayah, A., Pfeffer, M., Philipona, C. & Marquis-Weible, F. (1998) Chemically etched fibre tips for near-field optical microscopy: a process for smoother tips. *Appl. Opt.* **37**, 7289–7292.
- Levy, J., Nikitin, V., Kikkawa, J.M., Cohen, A., Samarth, N., Garcia, R. & Awschalom, D.D. (1996) Spatiotemporal near-field spin

- microscopy in patterned magnetic heterostructures. *Phys. Rev. Lett.* **76**, 1948–1951.
- Lewis, M.K., Wolanin, P., Gafni, A. & Steel, D.G. (1998) Near-field scanning optical microscopy of single molecules by femtosecond two-photon excitation. *Opt. Lett.* **23**, 1111–1114.
- Lienau, Ch., Richter, A., Behme, G. *et al.* (1998) Nanoscale mapping of confinement potentials in single semiconductor quantum wires by near-field optical spectroscopy. *Phys. Rev. B* **58**, 2045.
- Müller, R. & Lienau, C. (2000) Propagation of femtosecond optical pulses through uncoated and metal-coated near-field fibre probes. *Appl. Phys. Lett.* **76**, 3367–3369.
- Nechay, B.A., Siegner, U., Morier-Genoud, F., Schertel, A. & Keller, U. (1999) Femtosecond near-field optical spectroscopy of implantation patterned semiconductors. *Appl. Phys. Lett.* **74**, 61–63.
- Nötzel, R., Ramsteiner, M., Menniger, J., Trampert, A., Schönherr, H.-P., Däweritz, L. & Ploog, K.H. (1996) Micro-photoluminescence study at room temperature of sidewall quantum wires formed on patterned GaAs (311) A substrates by molecular beam epitaxy. *Jpn. J. Appl. Phys.* **35**, L297–L300.
- Pohl, D.W., Denk, W. & Lanz, M. (1984) Optical stethoscopy: image recording with resolution $\lambda/20$. *Appl. Phys. Lett.* **44**, 651–653.
- Richter, A., Behme, G., Süptitz, M. *et al.* (1997a) Real-space transfer and trapping of carriers into single GaAs quantum wires studied by near-field optical spectroscopy. *Phys. Rev. Lett.* **79**, 2145–2148.
- Richter, A., Süptitz, M., Lienau, C., Elsaesser, T., Ramsteiner, M., Nötzel, R. & Ploog, K.H. (1997b) Near-field optical spectroscopy of single GaAs quantum wires. *Surf. Interface Anal.* **25**, 583–592.
- Schmitt-Rink, S., Ell, C. & Haug, H. (1986) Many-body effects in the absorption, gain, and luminescence spectra of semiconductor quantum-well structures. *Phys. Rev. B* **33**, 1183–1189.
- Shah, J. (1999) *Ultrafast Spectroscopy of Semiconductors and Semiconductor Nanostructures* 2nd edn. Springer, Berlin.
- Smith, S., Holme, N.C.R., Orr, B., Kopelman, R. & Norris, T. (1998) Ultrafast measurement in GaAs thin films using NSOM. *Ultramicroscopy* **71**, 213–223.
- Stark, J.B., Mohideen, U., Betzig, E. & Slusher, R.E. (1996) Time-resolved non-linear near-field optical microscopy of semiconductor microdisks. *Ultrafast Phenomena IX* (ed. by J.-L. Martin, A. Migus, G.A. Mourou and A.H. Zewail), pp. 349–350. Springer Series in Chemical Physics, Springer, Berlin.